Computers and Concrete, *Vol. 24, No. 1 (2019) 73-83*
DOI: https://doi.org/10.12989/cac.2019.24.1.073

Effect of bond slip on the performance of FRP reinforced concrete columns under eccentric loading

Chunyang Zhu[1a], Li Sun[*1], Ke Wang[2], Yue Yuan[3] and Minghai Wei[1]

[1]Civil Engineering School, Shenyang Jianzhu University, Hunnan Road 9#, Shenyang,110168, China
[2]China Communications Construction Company First Highway Consultants Co. Ltd., Keji 2nd Road 63#, Xi'an 710075, China
[3]Highway Administration Bureau of Liaoning Communications Department, 13 Wei Road 19#, Shenyang 100168, China

(Received January 16, 2019, Revised May 1, 2019, Accepted June 4, 2019)

Abstract. Concrete reinforced with fiber reinforced polymer (FRP) bars (FRP-RC) has attracted a significant amount of research attention in the last three decades. A limited number of studies, however, have investigated the effect of bond slip on the performance of FRP-RC columns under eccentric loading. Based on previous experimental study, a finite-element model of eccentrically loaded FRP-RC columns was established in this study. The bondslip behavior was modeled by inserting spring elements between FRP bars and concrete. The improved Bertero-Popov-Eligehausen (BPE) bond slip model with the results of existing FRP-RC pullout tests was introduced. The effect of bond slip on the entire compression-bending process of FRP-RC columns was investigated parametrically. The results show that the initial stiffness of bond slip is the most sensitive parameter affecting the compression-bending performance of columns. The peak bond stress and the corresponding peak slip produce a small effect on the maximum loading capacity of columns. The bondslip softening has little effect on the compression-bending performance of columns. The sectional analysis revealed that, as the load eccentricity and the FRP bar diameter increase, the reducing effect of bond slip on the flexural capacity becomes more obvious. With regard to bond slip, the axial-force-bending-moment (P-M) interaction diagrams of columns with different FRP bar diameters show consistent trends. It can be concluded from this study that for columns reinforced with large diameter FRP bars, the flexural capacity of columns at low axial load levels will be seriously overestimated if the bond slip is not considered.

Keywords: FRP reinforced concrete; bond slip; compression-bending performance; P-M interaction diagram

1. Introduction

The feasibility of using fiber reinforced polymer (FRP) bars in reinforced concrete structures has been verified by extensive studies (Manalo and Benmokrane 2014, Kosmidou 2018, Lee 2018). Although the compressive strength of FRP bars is lower than their tensile strength, their application as compression longitudinal reinforcement can still achieve a certain strengthening effect (De Luca 2010, Tobbi 2012, Afifi 2013). However, at present, the design codes of various countries (ACI 440.1R-15, GB 50608-2010, CSA S 806-12 and JSCE-1997) offer very limited design guidelines for compression concrete members reinforced with FRP bars (FRP-RC) and the research in this area is not mature. Improving the study on compression performance of FRP-RC to realize its full structural potential is essential to solving the problem of durability for RC structures in highly corrosive environments.

Many investigations about the performance of FRP-RC columns under axial compression have been carried out (Hasan 2017, Sreenath 2017, Hadi 2016, 2017, Karim 2016, Tobbi 2013, Afifi 2013, Mohamed 2010, 2014, De Luca 2010, Sharbatdar 2003, Pessiki 1997). Regarding the aspect of compression-bending performance of FRP-RC, Peng *et al*. (2018) used OpenSees to establish a nonlinear model of eccentrically loaded FRP-RC columns, analyzing parametrically the second-order effects of eccentric loading on FRP-RC columns and obtaining a modified equation for the bending moment magnification factor. Hadhood *et al*. (2016, 2017) conducted experimental investigations on the eccentric loading performance of concrete columns reinforced with FRP bars and spirals. The axial force-moment (P-M) interaction diagrams were predicted based on the principles of strain compatibility and internal force equilibrium in accordance with the recommendations in the available design standards. Hadi*et al*. (2016, 2017) investigated GRFP reinforced concrete (GFRP-RC) and GFRP reinforced high-strength concrete (GFRP-HSC) columns. The experimental results show that the axial load and flexural capacity of the GFRP-RC columns are smaller than those of the steel reinforced concrete (steel-RC) columns. However, the ductility of the GFRP-RC columns was very close to that of the steel-RC columns. The ductility and post-peak axial load-axial deformation behavior of the GFRP-HSC specimens can be significantly improved by providing closely spaced helices. It also found that ignoring the contribution of the GFRP bars in compression leads to a considerable difference between analytical and experimental results. Zadeh *et al*. (2017)

*Corresponding author, Professor
E-mail: sunli2009@163.com
[a]Ph.D.
E-mail: cyzhu1087@163.com

ISSN: 1598-8198 (Print), 1598-818X (Online)

studied the influence of flexural stiffness and second-order effects on FRP-RC frames and discussed the practicality of the ACI 318 guidelines with respect to these two factors. The investigation conducted by Sreenath *et al.* (2017) revealed that the yield load and ultimate load at failure withstood by the steel-RC were considerably more than that of GFRP-RC. The energy absorption capacity of GFRP-RC was also poor compared to steel-RC columns. Both the columns exhibited nearly the same ductile behavior. Issa *et al.* (2012) explores the behavior of GFRP-RC and steel-RC columns subjected to eccentrically axial load. Large longitudinal deformations were recorded for columns with GFRP reinforcement and for columns with large tie spacing. However, tie spacing had no notable effect on the maximum lateral deflection and ductility of GFRP-RC columns. GFRP bars recorded higher strains than steel bars and these strains were larger when the tie spacing was large. The increase in the strength of the concrete was associated with reduction in the GFRP bar strain. Gong *et al.* (2009) systematically studied and summarized the characteristics of axial compression and the bending and seismic performance of FRP-RC columns and proposed corresponding design recommendations. Choo *et al.* (2006) studied the interaction and second-order effects of the P-M relationship of FRP-RC interface. The analytical results show that FRP-RC columns have a tendency to undergo brittle-tension failure. To avert brittle-tension failure to a failure controlled by concrete crushing, a reinforcement ratio that is greater than a minimum required reinforcement ratio is required. Sharbatdar *et al.* (2003) carried out experimental and analytical study on CFRP reinforced concrete (CFRP-RC) columns. It concluded that CFRP reinforced columns under combined axial and flexural stresses develop strengths that can be computed with plane section analysis similarly employed for steel-RC elements. Columns tested under monotonically increasing eccentric loading were able to develop their expected moment capacities. Mirmiran *et al.* (2001) proposed an FRP-RC design calculation method that considers second-order effects and is based on the bending moment magnification factor of reinforced concrete as specified by the ACI318-89 guidelines.

Another aspect to consider is the bond behavior between FRP bars and concrete, which is the main factor affecting the mechanical performance, failure mode, loading capacity, cracking width, deformation capacity, structural analysis and design of FRP-RC structural members. Xu *et al.* (2018) proposed and developed a piezoceramic-based active sensing approach to find the debonding between a GFRP bar and the concrete structure. Mohamed *et al.* (2017) used a novel beam-testing method to assess the bond performance of fiber-reinforced polymer (FRP) bars in reinforced-concrete resisting systems subjected to tension-compression reversed cyclic loading. Cyclic bond stress-slip relationship under different loading conditions was acquired. Mesbah *et al.* (2017) studied experimentally and numerically the evaluation of bond strength of FRP reinforcing rods in concrete. The effects of different parameters of FRP bar, such as type, shape and diameter, on the bond behavior of FRP rebar and concrete were evaluated. Vilanova *et al.* (2015) carried out Experimental study of bond-slip of GFRP bars in concrete under sustained

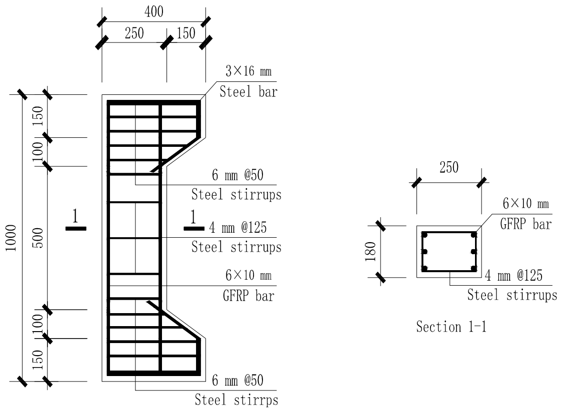

Fig. 1 Specimen design

loads. The distribution of bond stresses and their evolution during sustained loading were analyzed. Hao *et al.* (2007) carried out GFRP-RC bond-slip tests and examined how the bond-slip behavior is affected by such factors as reinforcement type and rib height, width, and spacing. Okelo *et al.* (2005) proposed an average bond strength equation that considers the effect of the type and anchorage length of FRP bars. Cosenza *et al.* (1997) summarized a large number of FRP bar bond-slip test results from earlier studies and analyzed the mechanism and influence of various factors, including fiber type, surface treatment methods, confining pressure, FRP bar diameter, and concrete strength, on bond-slip performance. Multiple studies have shown that, because the elastic modulus and surface hardness of FRP bars are generally lower than those of steel rebar, their performance with concrete is also inferior.

In FRP-RC beam-columns, the FRP-RC bond performance will affect the compression-bending performance when FRP bars are under tension. The aim of the present study is to clarify the effect of FRP-RC bond slip on the mechanical properties of FRP-RC columns under eccentric loading. Based on earlier experiments carried out by this research group, including FRP bar pull-out tests and eccentric compression test on FPR-RC short columns, the present study establishes a finite element model (FEM) and uses the improved Bertero-Popov-Eligehausen (BPE) bond-slip model (Cosenza *et al* 1997) to study the effect of bond slip on the entire eccentric loading process and the ultimate loading capacity of FRP-RC columns. The results of this study will give a theoretical reference for the design of FRP-RC beam-columns.

2. Establishment and verification of the FEM

2.1 Mechanical parameters of the model

An earlier experiment on the behavior of eccentrically loaded GFRP-RC columns is detailed elsewhere (Sun *et al.* 2017). The specimens were designed as compression members with small eccentricity, as shown in Fig. 1. The mechanical properties of the materials are as follows: GFRP bar diameter of 10 mm with rib spacing of 10 mm, tensile

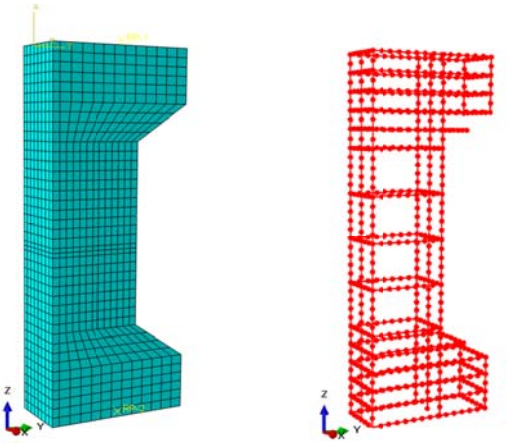

(a) Concrete (b) FRP reinforcement

Fig. 2 Finite-element meshing

elastic modulus of 92,400 MPa, tensile strength of 1103 MPa, compressive elastic modulus of 60,200 MPa, and compressive strength of 689 MPa. The concrete strength grade is C30, whereas the measured compressive resistance of the cubic specimens was 33.51 MPa. The load eccentricities of the specimens were *e*=75, 125 and 175 (mm), respectively.

To establish the FEM of eccentrically loaded GRFP-RC, the finite element software platform ABAQUS was used. The plastic damage model provided by ABAQUS material storage was adopted for concrete, whereas a linear elastic model was used for FRP bars. The detailed properties of each material were as follows: concrete elastic modulus of 30,000 MPa, a peak compressive resistance of 34 MPa, and a peak tensile strength of 2 MPa. In addition, the tensile and the compressive elastic modulus of the GRFP bars were 90,000 and 60,000 MPa, respectively. In addition, a three-dimensional eight-node element with reduced integration (C3D8R) was adopted for concrete, while a two-node 3D truss element (T3D2) was used for FRP bars. When the bond-slip relationship between FRP bars and concrete was not considered, the embedded constraint was used to model the interaction between the two materials. Finally, a mesh size sensitivity analysis was performed during the modeling process. The final meshing of the FEM is shown in Fig. 2.

2.2 Spring element

In finite element analyses, the cohesive surface interaction and the spring connection are two of the most common method to simulate the interface bond slip (Al-Osta 2018, Lezgy-Nazargah 2018). To simulate the bond-slip behavior between FRP bars and concrete, spring element connection was used in this study. Several groups of three-dimensional spring elements were evenly distributed along the FRP bars on the side opposite of the load. In each group, the two spring elements perpendicular to the specimen height were set as linear spring elements, while the elements along the specimen height were set as nonlinear spring elements. In an earlier pull-out test (Zhang 2016), the bonding stress versus relative slip (τ−s) relationship of GFRP-RC was obtained and used to describe

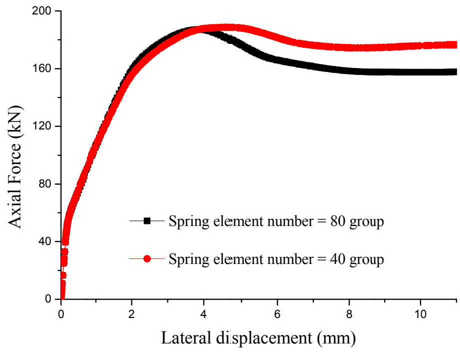

Fig. 3 Effect of the spring element number

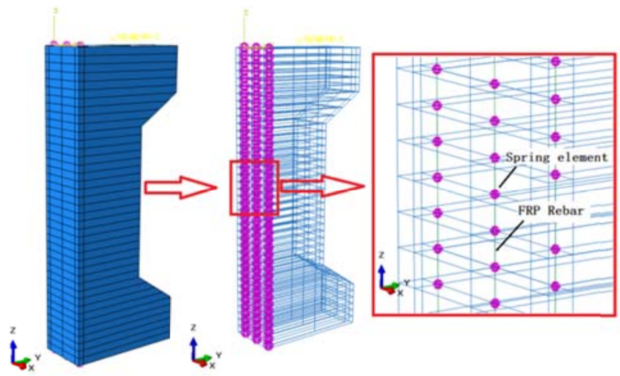

Fig. 4 Layout of spring elements

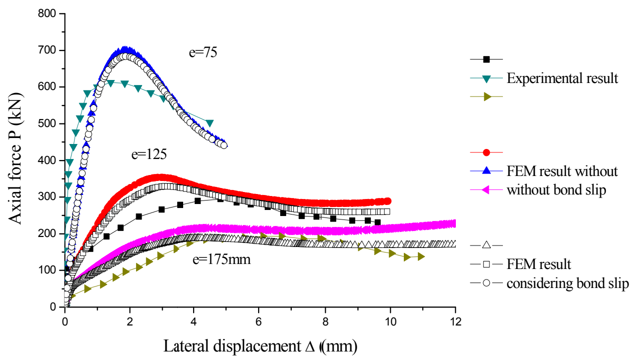

Fig. 5 Comparison of FEM and experimental results

the mechanical properties of the nonlinear spring elements. Fig. 3 shows the effect that the number of spring elements has on the finite-element calculation results. It is clear from Fig. 3 that the number of spring elements affects the calculation result, especially during the later stage of loading-that is, as the number of spring elements increases, the curve becomes more softening during the post-peak loading stage. During modeling, the spacing of spring elements matched the embedding length of FRP bars in the pull-out test, to avoid the error resulting from the effect of the embedding length on the bond-slip constitutive relationship. The detailed layout of spring elements is shown in Fig. 4.

2.3 Verification of the FEM results

Fig. 5 shows a comparison between the FEM and experimental results of FRP-RC column under eccentric

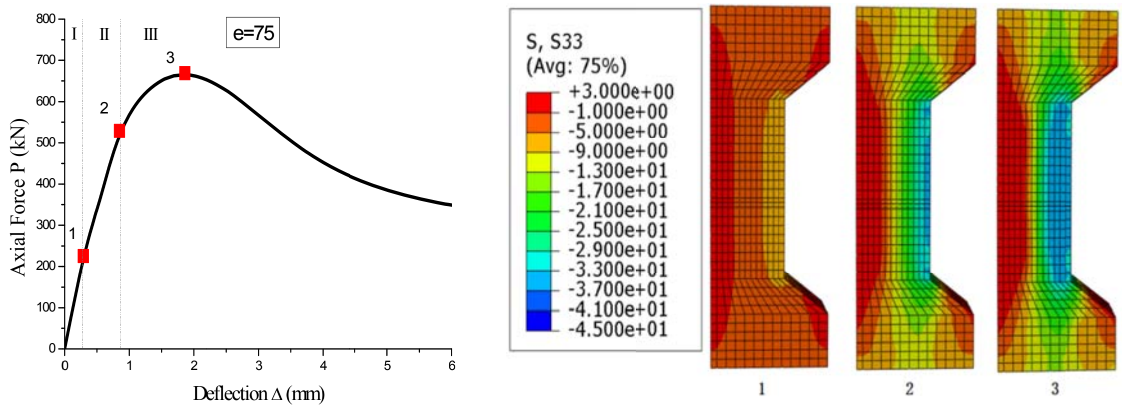

(a) e=75

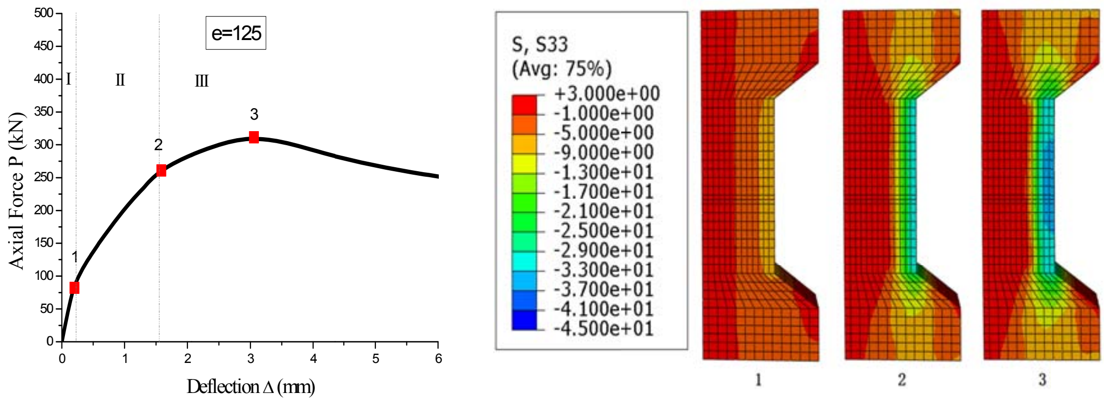

(b) e=125

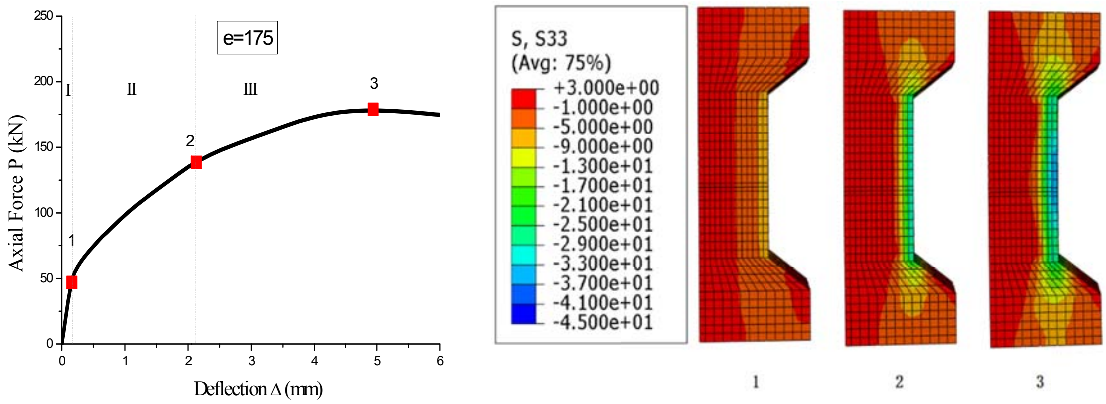

(c) e=175

Fig. 6 Stress contours corresponding to the characteristic points on the P–Δ curve

compression. It is clear that the initial stiffness and the maximum load calculated with the FEM are higher than those of the experimental results. However, the overall trends and key features of the simulated P–Δ curves are consistent with those obtained through experimental results. Considering the effect of bond slip, as the load eccentricity increases, the column stiffness decreases significantly, followed by a reduction of its loading capacity. The FEM results are in better agreement with the experimental results, compared with the case without bond slip.

3. Stress state corresponding to characteristic points on a P–Δ curve

It is evident from the experimental and FEM P–Δ curves that a typical curve can be divided into three bilinear-plus-nonlinear stages. This is consistent with the conclusions in previous work (Paramanantham 1994). This characteristic becomes more obvious as the load eccentricity increases. Fig. 6 shows the stress contours of concrete corresponding to the three stage-boundary points on the complete P–Δ curve, without considering the FRP bond-slip effect. It can be found that the decrease of stiffness at the transition (Point 1) from the stage I to the stage II is caused primarily by the cracking of concrete in the tension zone, whereas the further decrease of stiffness between the stage II and the stage III (Point 2) is caused by the obvious nonlinear behavior of concrete in the

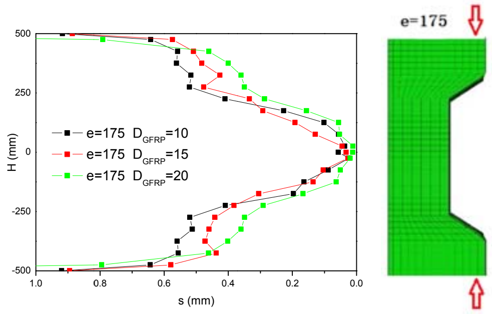

(a) FRP bar diameter effect

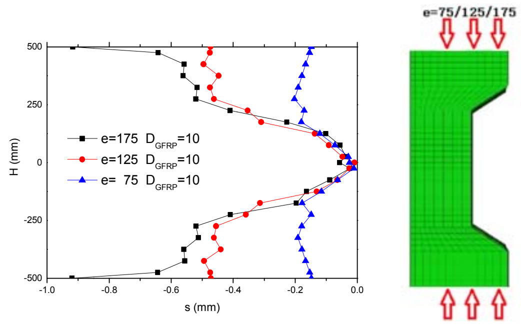

(b) Loading eccentricity effect

Fig. 7 Distribution of FRP bar-concrete relative slip along the specimen height

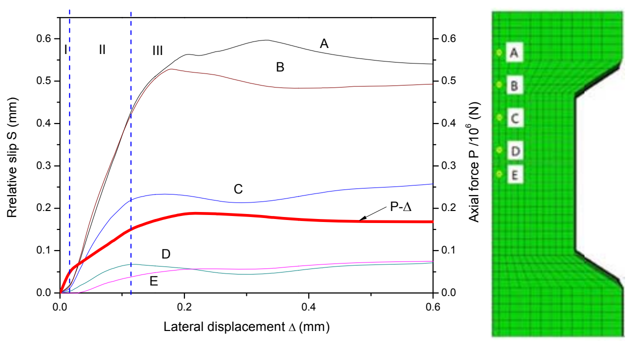

Fig. 8 Comparison of the FRP-RC S–Δ curve and the τ–s curve (specimen e=175)

compression zone. The peak value point (Point 3) is when some of the concrete in the compression zone reaches its peak compressive strength.

4. Distribution of concrete-FRP relative slip along the column height

For the FEMs considering bond slip, Fig. 7 shows the distribution of relative slip S between FRP bar and concrete along the specimen height when the column reaches its loading summit. It is clear that S is approximately symmetrical about the center of the specimen along its height-that is, S gradually increases from the center to both ends of the specimen. Fig. 7(a) shows that S tends to decrease gradually with the increase of the diameter of GFRP bar D_{GFRP}. S tends to increase significantly with the increase in the loading eccentricity e, as shown in Fig. 7(b).

Fig. 8 shows a comparison between the relative slip-lateral-displacement (S–Δ) at a few selected nodes (node A-E in Fig. 8) and the P–Δ curves in the FEM specimen e=175. Considering the three stages of the P–Δ curve mentioned above, the FRP-RC relative slip S remains within a small range (<0.025 mm) at stage I and increases rapidly at stage II. This is primarily because concrete cracks in the second loading stage and the equivalent plastic strain of concrete in FEM increases rapidly, resulting in a rapid increase of S. After reaching its peak value in the third stage, it is worth noting that S first drops slightly and then remains relatively stable hereafter, indicating that the bonding stress between GFRP bar and concrete keeps stable during the large deformation state. This is likely because the development of the concrete crack comes into a stable phase and FRP bars and concrete deform in coordination.

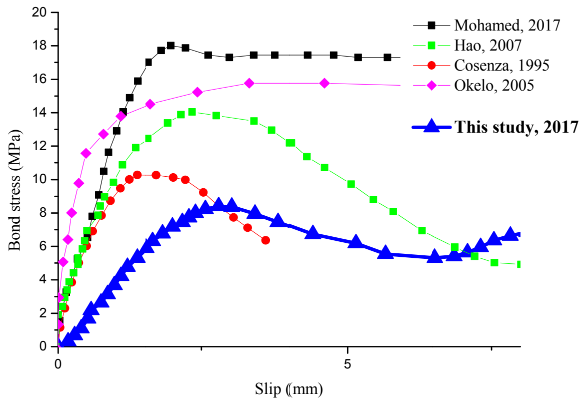

Fig. 9 Portion of the experimental τ–s results

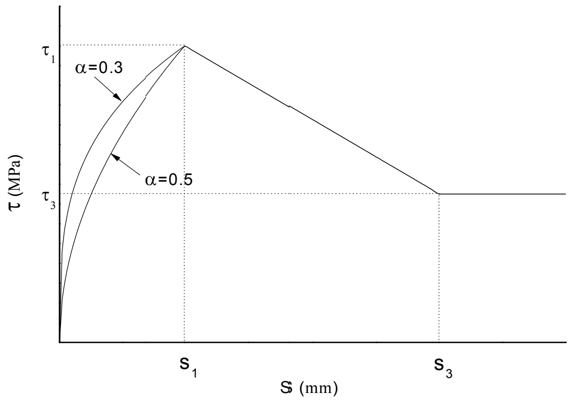

Fig. 10 Improved BPE model

5. Key parameters of the τ–s curve and their effect

To study the effect of bond slip on the compression-bending performance of FRP-RC columns, first, earlier FRP-RC pull-out experiments were reviewed. Fig. 9 shows the τ–s curves of several selected specimens from earlier experiments (Hao *et al.* 2007, Mohamed2017, Okelo *et al.* 2005, Cosenza *et al.* 1997). Because of the differences in FRP material properties (fiber or resin type), surface treatments (smooth, indented, and ribbed surface treatment), anchorage length and testing methods, significant variations can be noted in the bond-slip performance of different FRP

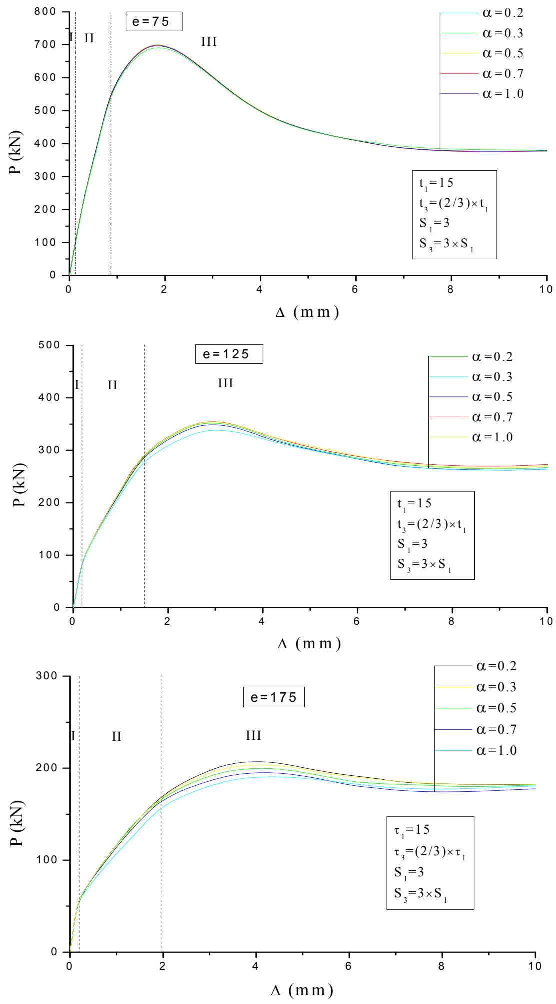

Fig. 11 Effect of parameter α

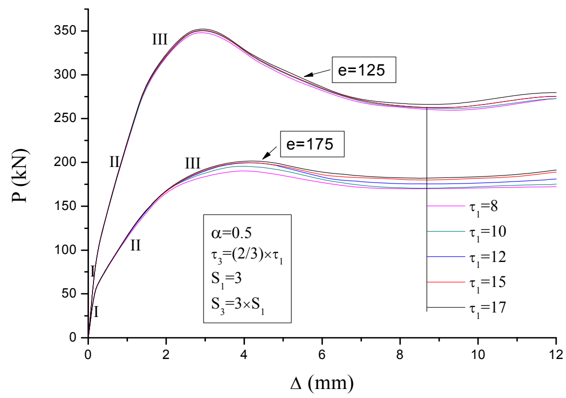

Fig. 12 Effect of parameter τ_1

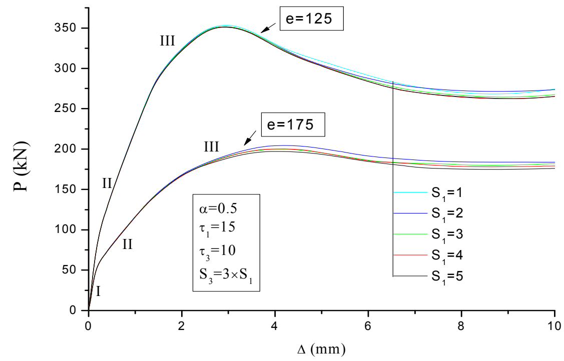

Fig. 13 Effect of parameter S_1

bars. These variations are manifested primarily in such aspects as bond-slip stiffness, the peak bond stress and its corresponding slip, and the residual bond stress. To study systematically the effect of bond-slip behavior on the performance of FRP-RC columns under eccentric loading, the present study carried out a finite-element parametric analysis based on the improved BPE bond-slip model (Cosenza *et al*. 1997). Eq. (1) shows the expression of improved BPE model.

$$\begin{aligned} &\text{Ascending segment:} \quad \tau/\tau_1 = (s/s_1)^{\alpha} && (s \le s_1) \\ &\text{Descending segment:} \quad \tau/\tau_1 = 1 - p(s/s_1 - 1) && (s_1 < s < s_3) \quad (1) \\ &\text{Residual stress segment:} \quad \tau = \tau_3 && (s > s_3) \end{aligned}$$

where τ_1 and s_1 are the maximum bond strength and the corresponding slip, respectively, τ_3 is the friction component of the bond resistance, and α, p are model parameters, which need to be determined from tests. Fig. 10 shows a typical τ–s curve from the improved BPE model.

Based on the collected existing experimental results, the model parameters were chosen as follows. The power index that determines the ascension of the curve in the initial loading stage is α=0.2−1.0, the peak bond stress τ_1=6−20 MPa and its corresponding peak slip s_1=0.5−4.0 mm, and the residual bond stress τ_3 was set to be equal to 20%-80% of τ_1.

5.1 Effect of the bond-slip Initial stiffness

In the improved BPE model, the change of power index α reflects the changes in the initial stiffness of the bond slip: as α decreases, the initial tangent modulus of the τ–s curve increases, and so does the corresponding initial stiffness of the bond slip. Fig. 11 shows the complete P−Δ curve of each specimen for different values of α.

It shows that α starts to affect the complete P−Δ curve approximately from stage II: the higher the initial stiffness of the bond-slip response, the higher the initial stiffness and loading capacity of the column. In addition, as the load eccentricity increases, the improvement of the stiffness and loading capacity of the column becomes more significant. During parameter analysis, when α was reduced by 80%, for the specimens with e=75, 125, and 175, the peak loading capacity improved by 1.4%, 5.1%, and 9.3%, respectively, and the tangent stiffness at the second stage of the P−Δ curve increased by 0.4%, 2.1%, and 13.6%, respectively.

5.2 Effect of the peak bond stress τ_1 and the corresponding peak slip S_1

Fig. 12 and Fig. 13 are the P−Δ curves for the e=125 and 175 specimens with various values of peak bond stress τ_1 and its corresponding peak slip S_1.

Unlike α, parameters τ_1 and S_1 produce significant

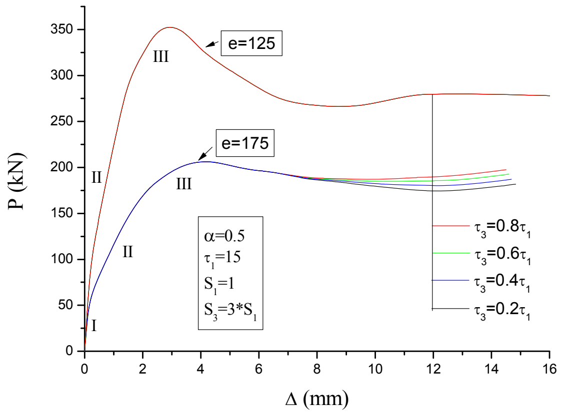

Fig. 14 Effect of parameter τ_3

influence in stage III of the P–Δ curve-that is, during its obviously nonlinear stage. As τ_1 increases and S_1 decreases, the eccentric loading capacity gradually decreases. This pattern becomes even more obvious with the increase of eccentricity. This shows that the lower the peak secant stiffness of bond slip (the slope of the line connecting the origin with the peak value of the τ–s curve), the more obvious the decrease in eccentric loading performance of the specimens. However, if the boundary point (point 2) between the second and the third stages of the P–Δ curve is used as a design point of a structural component, then the peak bond stress and its corresponding peak slip has no significant effect on the normal performance of such a structural component.

5.3 Effect of the residual bonding stress τ_3

The parameter τ_3 controls the residual bond strength and the stiffness during the softening stage of the τ–s curve. Fig. 14 shows the P–Δ curves obtained by changing the value of τ_3 in the FEM. For the specimen with eccentricity e=125, the change in τ_3 has not resulted in any change of the P–Δ curve, whereas, for the e=175 specimen, the increase of τ_3 has only resulted in the loading improvement in last curve segment. Further analysis has revealed that, if S_1 is further reduced, the influence point of τ_3 on the P–Δ curve will advance slightly, but it will not exceed the peak value point of the P–Δ curve, indicating that the softening behavior of the bond slip tends to not affect the loading performance in the normal service state.

6. Effect of bond slip on loading capacity

6.1 Effect of the FRP bar diameter on loading

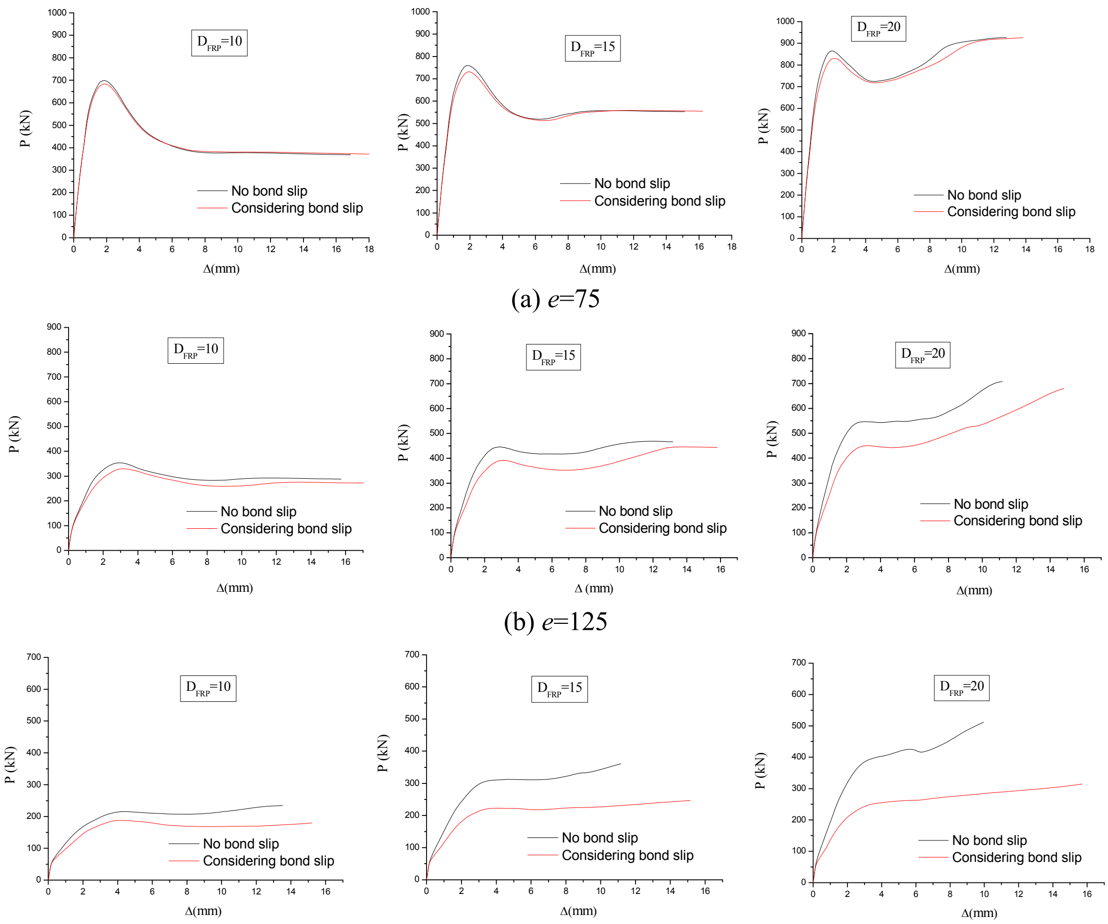

(a) e=75

(b) e=125

(c) e=175

Fig. 15 Effect of bond slip on compression-bending performance under different FRP bar diameter conditions

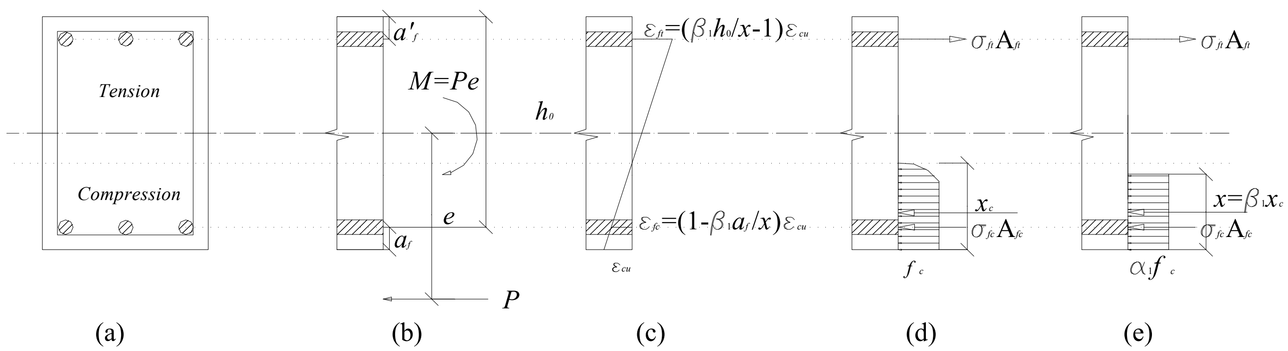

Fig. 16 Cross sectional analysis model (a) typical cross section; (b) cross section load; (c) strain compatibility; (d) generalized stress block; (e) equivalent rectangular stress block

Adjusting the FRP bar diameters in the FEM enabled the P−Δ curves of FRP-RC columns with FRP bar diameters of D_{FRP}=10/15/20 (mm), under a no bond slip condition and considering bond slip, to be obtained and compared, as shown in Fig. 15. The effect of FRP bar diameter on bond slip was not considered during the analyses. Previous studies (Hao 2007, Zhang 2015, Okelo 2005 and Cosenza 1997) show that, the bond strength decreases as the bar diameter increases. In fact, the impact of bond slip on the eccentric loading performance of columns would be overestimated when the effect of the FRP bar diameter increase is not considered, resulting in conservative analytical results in this analyses. The finite element results show the loading capacity of columns gradually increases and the post peak degradation of loading capacity decreases with the increasing diameter of FRP bars. Moreover, it is worth noting from Fig. 15 that the weakening effect of FRP-RC bond slip on the stiffness and loading capacity of columns becomes even more obvious as the FRP bar diameter increases.

6.2 Analysis of P-M interaction diagram

Based on the preceding FEM analysis of columns with different FRP bar diameters and loading eccentricities, the corresponding *P-M* interaction diagrams were obtained. Cross sectional analysis (Fig. 16) was conducted and the theoretical *P-M* interaction diagram was obtained by using Eq. (2).

$$
\begin{aligned}
&\sigma_{ft} = \varepsilon_{cu}(\frac{\beta_1 h_0}{x} - 1)E_{ft} \\
&\sigma_{fc} = \varepsilon_{cu}(1 - \frac{\beta_1 a_f}{x})E_{fc} \\
&P = \alpha_1 f_c bx - \sigma_{ft}A_{ft} + \sigma_{fc}A_{fc} \\
&M = \alpha_1 f_c bx(h_0 - \frac{x}{2}) + \sigma_{fc}A_{fc}(h_0 - a_f) - P(\frac{h}{2} - a_f)
\end{aligned} \tag{2}
$$

Where σ_{ft} and σ_{fc} are the tensile and compressive stress of FRP bar, respectively. ε_{cu} is the ultimate strain of concrete. E_{ft} and E_{fc} are the tensile and compressive elastic modulus of FRP bar, respectively. A_{ft} and A_{fc} are the cross-sectional area of the tensile and compressive FRP bars, respectively. f_c is the summit strength of concrete. x is the compression depth of concrete. α_1 and β_1 is the equivalent

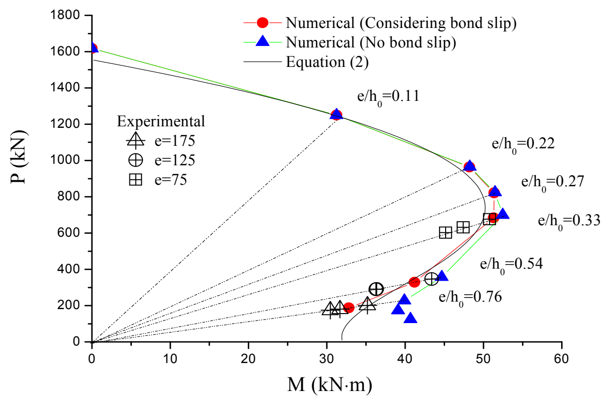

Fig. 17 Comparison of the theoretical/FEM P-M interaction diagrams and experimental results

rectangular stress diagram coefficient, α_f and h_0 are the distance from the centroid of FRP bar to the near and far edge of the cross section, respectively, as shown in Fig. 16.

The theoretical and FEM P-M interaction diagram and experimental results are compared in Fig. 17. It is evident that they are in good agreement. Furthermore, when the FRP-RC bond slip is considered, the FEM results are even closer to the experimental results.

Fig. 18 shows a comparison of FEM *P-M* interaction diagrams, with and without consideration of bond slip, and for varying FRP bar diameters. It shows that, when the load eccentricity e is small, FRP-RC bond slip produces no effect on the axial loading capacity and flexural capacity, primarily because FRP bars are under compression. However, if the eccentricity that corresponds to the FRP bar at the beginning of tension was used as a limit e_c, when e exceeds e_c and increases gradually, the weakening effect on flexural capacity caused by bond slip becomes even more obvious. Moreover, the flexural capacity reduction is magnified as the FRP bar diameter D_{FRP} increases, causing large deviations in *P-M* interaction diagrams with and without consideration of bond slip, as shown in Fig. 18.

It can be concluded that, if the bond slip is not considered during the design process, the flexural capacity of columns reinforced with large diameter FRP bars will be seriously overestimated at the low axial load levels.

The FEM calculation results show that, when the effect of bond slip is not considered, as the FRP diameter increases, the *P-M* interaction curve changes

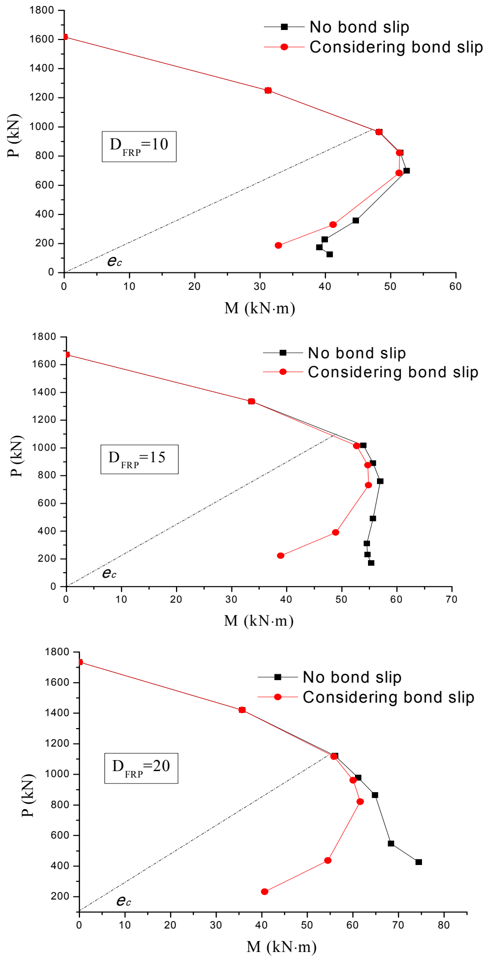

Fig. 18 Effect of bond slip on *P-M* curves with different FRP bar diameters

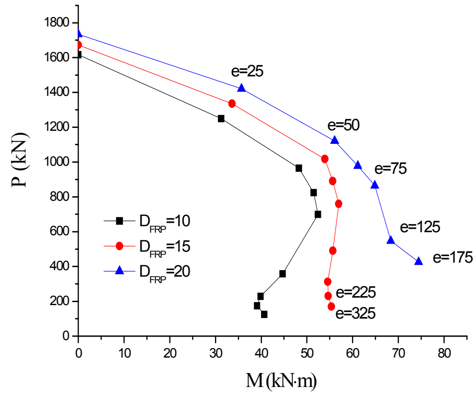

(a) Without bond slip

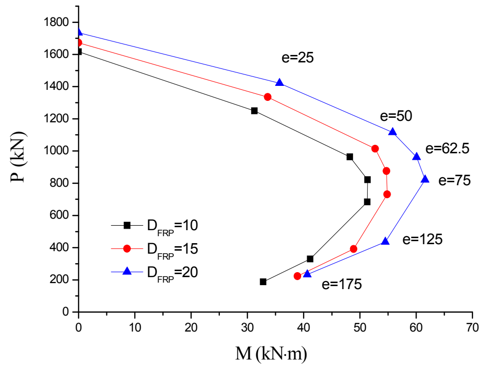

(b) Considering bond slip

Fig. 19 Effect of bond slip on P-M curves with different FRP bar diameters

correspondingly. That is, when the reinforcement ratio is low, the *P-M* interaction curve is a nonmonotonic curve with an inflection point, as exhibited by the D_{FRP}=10 curve in Fig. 19(a). However, as the FRP reinforcement ratio increases, the curve becomes monotonic and the inflection point disappears gradually, as exhibited by the D_{FRP}=20 curve in Fig. 19(a), which is consistent with the previous findings of Hadhood *et al*. (2016).

However, when the effect of the bond slip is considered, the trends of the P-M curves for columns with different FRP bar diameters are consistent; all become nonmonotonic and approach the curve with a low FRP bar diameter, as shown in Fig. 19(b), which reflects the fact that as the FRP bar diameter increases, the weakening effect of the bond slip on column flexural capacity increases at low axial load levels.

7. Conclusions

In this study, the compression-bending performance of FRP-RC columns with consideration of bond slip was carried out using finite-element analysis. Moreover, the effects of key parameters of the bond-slip constitutive model on the compression-bending performance and the loading capacity of FRP-RC columns were discussed. Within these parameters, the main findings of this study are as follows.

During eccentric compression, FRP-RC columns undergo two obvious stiffness degradation stages, the first due to concrete cracking in the tension zone and second due to the significant nonlinear behavior of concrete in the compression zone.

The initial stiffness of bond slip is the main factor affecting the mechanical performance of FRP-RC columns under eccentric loading. The higher the initial stiffness of the bond slip, the higher the stiffness and loading capacity of the column.

The peak bond stress and its corresponding peak slip had an insignificant effect on the stiffness, but they had a small effect on summit loading capacity. The softening behaviour of bond slip only affects the performance of columns under large-deformation conditions, whereas it has little effect on the normal performance of structural components.

Regarding the loading capacities reflected in *P-M* interaction diagrams, the load eccentricity when tension occurs in the FRP bar can be used as a limit. The weakening action of bond slip on the compression-bending performance becomes more evident when the eccentricity rate exceeds the limit. Moreover, as the FRP bar diameter increases, the degradation of column stiffness and loading capacity also increases. With respect to FRP-RC bond slip, the *P-M* interaction diagrams of columns with different FRP bar diameter have consistent trends.

In cases of eccentrically loading column with large eccentricity or high FRP bar diameter, bond slip has a significant weakening effect on the flexural capacity at low axial load levels. This effect should be carefully considered in practical engineering applications.

Acknowledgments

The research described in this paper was financially supported by National Natural Science Foundation of China, grant number “51878420” and “51578347” and National Key Research and Development Program of China, grant number “2018YFC1504303”.

References

ACI 440.1R-15 (2015), Guide for the Design and Construction of Structural Concrete Reinforced with Fiber-Reinforced Polymer (FRP) Bars, ACI Committee, Farmington Hills, MI, USA.

Afifi, M.Z., Mohamed, H.M. and Benmokrane, B. (2014), “Axial capacity of circular concrete columns reinforced with GFRP bars and spirals”, *J. Compos. Constr.*, **18**(1), 04013017. https://doi.org/10.1061/(ASCE)CC.1943-5614.0000438.

Afifi, M.Z., Mohamed, H.M. and Benmokrane, B. (2014), “Strength and axial behavior of circular concrete columns reinforced with CFRP bars and spirals”, *J. Compos. Constr.*, **18**(2), 04013035. https://doi.org/10.1061/(ASCE)CC.1943-5614.0000430.

Al-Osta, M.A., Al-Sakkaf, H.A., Sharif, A.M., Ahmad, S. and Baluch, M.H. (2018), “Finite element modeling of corroded RC beams using cohesive surface bonding approach”, *Comput. Concrete*, **22**(2), 167-182. https://doi.org/10.12989/cac.2018.22.2.167.

Choo, C.C., Harik, I.E. and Gesund, H. (2006), “Minimum reinforcement ratio for fiber-reinforced polymer reinforced concrete rectangular columns”, *ACI Mater. J.*, **103**(3), 460.

Choo, C.C., Harik, I.E. and Gesund, H. (2006), “Strength of rectangular concrete columns reinforced with fiber-reinforced polymer bars”, *ACI Struct. J.*, **103**(3), 452.

Cosenza, E., Manfredi, G. and Realfonzo, R. (1997), “Behavior and modeling of bond of FRP rebars to concrete”, *J. Compos. Constr.*, **1**(2), 40-51. https://doi.org/10.1061/(ASCE)1090-0268(1997)1:2(40).

CSA S806-12(2012), Design and Construction of Buildings Components with Fiber-reinforced Polymers, Canadian Standards Association (CSA), Toronto, Ontario, Canada.

De Luca, A., Matta, F. and Nanni, A. (2010), “Behavior of full-scale glass fiber-reinforced polymer reinforced concrete columns under axial load”. *ACI Struct. J.*, **107**(5), 589. https://doi.org/10.14359/51663912.

GB 50608-2010 (2010), Technical Code for Infrastructure Application of FRP Composites, Ministry of Housing and Urban-Rural Development of the People’s Republic of China, Beijing, China.

Gong, Y. and Zang J.W. (2009), “Experimental study of reinforced concrete eccentric compression column with CFRP tendons”, *China Civil Eng. J.*, **42**(10), 46-52. https://doi.org/10.1007/978-3-540-85168-4_52.

Hadhood, A., Mohamed, H.M. and Benmokrane, B. (2016), “Axial load-moment interaction diagram of circular concrete columns reinforced with CFRP bars and spirals: Experimental and theoretical investigations”, *J. Compos. Constr.*, **21**(2), 04016092. https://doi.org/10.1061/(ASCE)CC.1943-5614.0000748.

Hadhood, A., Mohamed, H.M. and Benmokrane, B. (2016), “Experimental study of circular high-strength concrete columns reinforced with GFRP bars and spirals under concentric and eccentric loading”, *J. Compos. Constr.*, **21**(2), 04016078. https://doi.org/10.1061/(ASCE)CC.1943-5614.0000734.

Hadhood, A., Mohamed, H.M. and Benmokrane, B. (2017), “Failure envelope of circular concrete columns reinforced with glass fiber-reinforced polymer bars and spirals”, *ACI Struct. J.*, **114**(6), 1417-1428. https://doi.org/10.14359/51689498.

Hadhood, A., Mohamed, H.M. and Benmokrane, B. (2017), “Strength of circular HSC columns reinforced internally with carbon-fiber-reinforced polymer bars under axial and eccentric loads”, *Constr. Build. Mater.*, **141**, 366-378. https://doi.org/10.1016/j.conbuildmat.2017.02.117.

Hadhood, A., Mohamed, H.M., Ghrib, F. and Benmokrane, B. (2017), “Efficiency of glass-fiber reinforced-polymer (GFRP) discrete hoops and bars in concrete columns under combined axial and flexural loads”, *Compos. Part B: Eng.*, **114**, 223-236. https://doi.org/10.1016/j.compositesb.2017.01.063.

Hadi, M.N. and Youssef, J. (2016), “Experimental investigation of GFRP-reinforced and GFRP-encased square concrete specimens under axial and eccentric load, and four-point bending test”, *J. Compos. Constr.*, **20**(5), 04016020. http://dx.doi.org/10.1061/(ASCE)CC.1943-5614.0000675.

Hadi, M.N., Hasan, H.A. and Sheikh, M.N. (2017), “Experimental investigation of circular high-strength concrete columns reinforced with glass fiber-reinforced polymer bars and helices under different loading conditions”, *J. Compos. Constr.*, **21**(4), 04017005. http://dx.doi.org/10.1061/(ASCE)CC.1943-5614.0000784

Hadi, M.N., Karim, H. and Sheikh, M.N. (2016), “Experimental investigations on circular concrete columns reinforced with GFRP bars and helices under different loading conditions”, *J. Compos. Constr.*, **20**(4), 04016009. http://dx.doi.org/10.1061/(ASCE)CC.1943-5614.0000670.

Hao, Q.D., Wang, Y.L., Zhang, Z.C. and Ou, J.P. (2007), “Bond strength improvement of GFRP rebars with different rib geometries”, *J. Zhejiang Univ.-Sci. A*, **8**(9), 1356-1365.https://doi.org/10.1631/jzus.2007.a1356.

Hasan, H.A., Sheikh, M.N. and Hadi, M.N. (2017), “Performance evaluation of high strength concrete and steel fiber high strength concrete columns reinforced with GFRP bars and helices”, *Constr. Build. Mater.*, **134**, 297-310. https://doi.org/10.1016/j.conbuildmat.2016.12.124.

Issa, M., Metwally, I. and Elzeiny, S. (2012), “Performance of eccentrically loaded GFRP reinforced concrete columns”, *World J. Eng.*, **9**(1), 71-78. https://doi.org/10.1260/1708-5284.9.1.71.

JSCE (1997), Recommendation for Design and Construction of Concrete Structures using Continuous Fiber Reinforcing Materials, Japan Society of Civil Engineers, Tokyo, Japan.

Karim, H., Sheikh, M.N. and Hadi, M.N. (2016), “Axial load-axial deformation behaviour of circular concrete columns reinforced with GFRP bars and helices”, *Constr. Build. Mater.*, **112**, 1147-1157. https://doi.org/10.1016/j.conbuildmat.2016.02.219.

Kosmidou, P.M.K., Chalioris, C.E. and Karayannis, C.G. (2018), “Flexural/shear strength of RC beams with longitudinal FRP bars an analytical approach”, *Comput. Concrete*, **22**(6), 573-592. https://doi.org/10.12989/cac.2018.22.6.573.

Lee, S.J., Moon, D.Y., Ahn, C.H., Lee, J.W. and Zi, G. (2018), “A precast slab track partially reinforced with GFRP rebars”, *Comput. Concrete*, **21**(3), 239-248. https://doi.org/10.12989/cac.2018.21.3.239.

Lee, Y.H., Kim, M.S., Kim, H., Lee, J. and Kim, D.J. (2013), “Experimental study on bond strength of fiber reinforced polymer rebars in normal strength concrete”, *J. Adhes. Sci. Technol.*, **27**(5-6), 508-522.

https://doi.org/10.1080/01694243.2012.687554.

Lezgy-Nazargah, M., Dezhangah, M. and Sepehrinia, M. (2018), “The effects of different FRP/concrete bond-slip laws on the 3D nonlinear FE modeling of retrofitted RC beams-A sensitivity analysis”, *Steel Compos. Struct.*, **26**(3), 347-360. https://doi.org/10.12989/scs.2018.26.3.347.

Manalo, A., Benmokrane, B., Park, K.T. and Lutze, D. (2014), “Recent developments on FRP bars as internal reinforcement in concrete structures”, *Concrete Aust.*, **40**(2), 46-56.

Mesbah, H.A., Benzaid, R. and Benmokrane, B. (2017), “Evaluation of bond strength of FRP reinforcing rods in concrete and FE modeling”, *Int. J. Civil Eng. Constr. Sci.*, **4**(3), 21-41.

Mirmiran, A., Yuan, W. and Chen, X. (2001), “Design for slenderness in concrete columns internally reinforced with fiber-reinforced polymer bars”, *Struct. J.*, **98**(1), 116-125. https://doi.org/10.14359/10153.

Mohamed, H.M. and Masmoudi, R. (2010), “Axial load capacity of concrete-filled FRP tube columns: Experimental versus theoretical predictions”, *J. Compos. Constr.*, **14**(2), 231-243. https://doi.org/10.1061/(ASCE)CC.1943-5614.0000066.

Mohamed, H.M., Afifi, M.Z. and Benmokrane, B. (2014), “Performance evaluation of concrete columns reinforced longitudinally with FRP bars and confined with FRP hoops and spirals under axial load”, *J. Bridge Eng.*, **19**(7), 04014020. https://doi.org/10.1061/(ASCE)BE.1943-5592.0000590.

Mohamed, N., Farghaly, A.S. and Benmokrane, B. (2017), “Beam-testing method for assessment of bond performance of FRP bars in concrete under tension-compression reversed cyclic loading”, *J. Compos. Constr.*, **21**(1), 06016001. https://doi.org/10.1061/(ASCE)CC.1943-5614.0000687.

Okelo, R. and Yuan, R.L. (2005), “Bond strength of fiber reinforced polymer rebars in normal strength concrete”, *J. Compos. Constr.*, **9**(3), 203-213. https://doi.org/10.1016/j.conbuildmat.2008.04.011.

Paramanantham, N.S. (1994), “Investigation of the behavior of concrete columns reinforced with fiber reinforced plastic rebar”, Ph.D. Dissertation, Lamer University, Beaumont, Texas.

Peng, F. and Xue, W.C. (2018), “Calculation approach of ultimate capacity of FRP reinforced concrete columns under eccentric compression”, *J. Build. Struct.*, **39**, 147-155. https://doi.org/10.14006/j.jzjgxb.2018.10.017.

Pessiki, S. and Pieroni, A. (1997), “Axial load behavior of large-scale spirally-reinforced high-strength concrete columns”, *ACI Struct. J.*, **94**(3), 304-314. https://doi.org/10.1016/S0925-8388(97)00116-3.

Sharbatdar, M.K. (2003), “Concrete columns and beams reinforced with FRP bars and grids under monotonic and reversed cyclic loading”, Ph.D. Dissertation, University of Ottawa, Ottawa.

Sreenath, S., Balaji, S. and Raja Mohan, K.S. (2017), “Behaviour of axially and eccentrically loaded short columns reinforced with GFRP bars”, *IOP Conf. Ser.: Earth Environ. Sci.*, **80**, 012030. https://doi.org/10.1088/1755-1315/80/1/012030.

Sun, L. and Wei, M. (2017), “Experimental study on the behavior of GFRP reinforced concrete columns under eccentric axial load”, *Constr. Build. Mater.*, **152**, 214-225. https://doi.org/10.1016/j.conbuildmat.2017.06.159.

Tobbi, H., Farghaly, A. S. and Benmokrane, B. (2013), “Behavior of concentrically loaded fiber-reinforced polymer reinforced concrete columns with varying reinforcement types and ratios”, *ACI Struct. J.*, **111**(2), 375-385. https://doi.org/10.14359/51686528.

Tobbi, H., Farghaly, A.S. and Benmokrane, B. (2012), “Concrete columns reinforced longitudinally and transversally with glass fiber-reinforced polymer bars”, *ACI Struct. J.*, **109**(4), 551-558. https://doi.org/10.14359/51683874.

Tobbi, H., Farghaly, A.S. and Benmokrane, B. (2013), “Strength model for concrete columns reinforced with fiber-reinforced polymer bars and ties”, *ACI Struct. J.*, **1114**, 789-798. https://doi.org/10.14359/51686630.

Vilanova, I., Baena, M., Torres, L. and Barris, C. (2015), “Experimental study of bond-slip of GFRP bars in concrete under sustained loads”, *Compos. Part B: Eng.*, **74**, 42-52. https://doi.org/10.1016/j.compositesb.2015.01.006.

Xu, K., Ren, C., Deng, Q., Jin, Q. and Chen, X. (2018), “Real-time monitoring of bond slip between GFRP bar and concrete structure using piezoceramic transducer-enabled active sensing”, S*ensor.*, **18**(8), 2653. https://doi.org/10.3390/s18082653.

Zadeh, H.J. and Nanni, A. (2017), “Flexural stiffness and second-order effects in fiber-reinforced polymer-reinforced concrete frames”, *ACI Struct. J.*, **114**, 533-543. https://doi.org/10.14359/51689257.

Zhang, Y. (2016), “Experimental study on bond performance theory between GFRP bar and concrete”, Master’s Dissertation, Shenyang Jianzhu University, Shenyang.

CC